PCCP

Cite this: *Phys. Chem. Chem. Phys.*, 2011, **13**, 19214–19225

www.rsc.org/pccp

PERSPECTIVE

Functional noble metal nanoparticle superlattices grown at interfaces

Keisaku Kimura*[a] and Thalappil Pradeep*[b]

Received 13th July 2011, Accepted 7th September 2011
DOI: 10.1039/c1cp22279a

Nanoparticle crystals or superlattices (SLs) are three dimensional arrangements of nanoparticles in the micrometre regime. In SLs, the particles are periodically arranged in a coherent long range order and hence they show collective properties. Various spectroscopic, scattering and imaging techniques have been used to understand the structure of self-assembled SLs. Extensive interest in particle SLs is due to the collective properties of the building blocks, which help us to understand the evolution in properties of organized structures. Controlling the assembly of such organized solids may open up new opportunities for fundamental studies as well as for engineering advanced materials with useful attributes. This review presents our efforts in creating SLs of noble metal nanoparticles and studies performed with those materials.

1. Introduction

Self-organized structures of nanoparticles, called nanoparticle crystals or superlattices (SLs), belong to a new class of materials.[1–4] The term SL brings to mind periodic nanometre thin layers of two or more materials, often made with semiconductors, leading to quantum well structures. Such structures exhibit multiple periodicity and the nanoparticle crystals discussed here too exhibit this attribute. Just as assembly of atoms and molecules leads to crystals, similar organization of nanoparticles leads to nanoparticle crystals. This review is on the creation of noble metal SLs by the chemical interaction of monolayers and inducing properties in such materials through selective functionalization of the monolayers.[5,6] Important aspects of self-organization of particles are their similarity and complementarity; here similarities in size, shape and functionality are considered. In this discussion, principally based on our own work, we are concerned with spherical nanoparticles alone, although

[a] *Graduate School of Material Science, University of Hyogo, Hyogo 678-1297, Japan. E-mail: kimura@sci.u-hyogo.ac.jp*
[b] *DST Unit of Nanoscience, Indian Institute of Technology, Madras 600036, India. E-mail: pradeep@iitm.ac.in*

Keisaku Kimura

K. Kimura received his PhD degree in Chemistry at the University of Tokyo in 1973 and was a research associate at the Institute for Molecular Science, where he was engaged in the research of the solid state properties of metallic ultrafine particles dispersed in organic solvents. He was a professor at University of Hyogo for 20 years and had been a Director of Central Library and a Dean of Faculty of Science and Graduate School of Science. He obtained a distinguished visiting professor position from Universite Pierre et Marie Curie, in Paris, France, in 2009. He is now a Professor Emeritus at University of Hyogo. His research interests include construction of three-dimensional particle crystals, characterization of these 3D materials by transmission electron microscopy and scanning electron microscopy, optical and transport properties of nano-size materials, and preparation of metallic nanoparticle–protein hybrids.

Thalappil Pradeep

T. Pradeep earned his PhD from the Indian Institute of Science in 1991 and had post doctoral training at the Lawrence Berkeley Laboratory, University of California, Berkeley and Purdue University, West Lafayette. He held visiting positions at several universities and institutes in Asia and Europe. His research interests are in nanomaterials, molecular surfaces, monolayers, ion/surface collisions, clusters, spectroscopy, electronic structure and instrumentation. His principal research theme is around molecular materials. He is committed to finding affordable solutions for drinking water for the poor. One of his technologies has been commercialized. He is the author of the introductory textbook Nano: The Essentials (McGraw-Hill) and is one of the authors of the monograph Nanofluids (Wiley-Interscience). He is a Fellow of the Indian Academy of Sciences. His other interests include education, popularization of science and development of advanced teaching aids.

self-organization of anisotropic nanostructures has also been reported. Self-assembled structures of magnetic,[7,8] semiconducting[9–14] and mixed particles[15,16] are known as also anisotropic nanostructures involving these materials.[17–19] Our discussion will be limited to noble metal nanoparticles, although we refer to the earlier work of metal nanoparticles in general.

Among motivations of research in nanoscience and nanotechnology is the realization of unconventional physico-chemical properties when bulk materials are finely divided to form ultrafine particles or quantum dots in the size regime of nanometres. In this state, the particles produced must be suspended in solvents or buried in solid matrices or flown in gas streams to avoid unintended contact between themselves or with the surfaces of the container to avoid spontaneous coalescence. Hence it is inherently impossible to build useful devices and exotic materials using these particles. One way to prevent such coalescence is by introducing surface modifier molecules or creating an oxidized layer. The latter is achieved by mild oxidation and was applied to Fe, Co, and Ni alloy nanoparticles of 15 nm diameter produced by a gas-evaporation technique.[20] The formed nano-metal powder was not stable when deposited into liquid. Hence it is necessary to synthesize nano-metal particles in a dispersed liquid phase with stabilized surfaces. The traditional approach to prepare metallic nano-particles in aqueous suspension is by the reduction of metal salts using citrate or succinate anions.[21] However, irreversible coagulation takes place upon drying these sols. It is impossible to stock these particles in the dry state, preventing further handling and examination. To get larger quantities of materials, we need to separate the formed particles from the growing phase. One of the prominent methods is the phase transfer route devised by Brust *et al.*[22] in oily solutions and the other is the phase separation method by Schaaff and Whetten[23] and ours[24,25] in aqueous solutions. The reverse micelle method was reported by Taleb and Pileni.[4,26] Surface modifier molecules could be phosphine derivatives, carboxylic acid, amines and thiols. The types of ligands vary depending on the nature of metallic nanoparticles. The water dispersible nanoparticles have special advantages: (1) hydrogen bond mediation, (2) affinity to biomaterials, and (3) availability of many kinds of separation methods developed in biochemistry and biology. However, the aqueous phase limits the type of modifier molecules which can be used.

Since Brust *et al.*'s discovery of a two dimensional (2D) SL made of thiolate protected gold nanoparticles grown from toluene solutions,[27] there have been a number of reports on the formation of noble metal-superlattices from colloidal dispersions. Many of these are confined to oily dispersions and less work was done on aqueous solutions, in which we can control several parameters such as pH, electrolyte species, ionic strength, *etc*. accurately to assist the self-assembly process. Furthermore, aqueous system is very important in biological functions and applications to keep the process environment friendly. In this review, we describe the concept of the phase separation method and its application for the preparation of nanoparticles with hydrophilic surfaces. In addition, we show the characteristics and functions of SLs formed at *gas/liquid interfaces*. Our work has been on three dimensional, isolable particle crystals of tens of micrometres in dimensions and we will not be discussing 2D SLs formed on substrates such as transmission electron microscopy (TEM) grids.

2. Surface modification and self-organization

(a) Surface modification of particles

Synthesis. We used 4 kinds of carboxyl thiols as shown in Scheme 1 as hydrophilic agents. Since carboxylic acids form closed or open dimers through hydrogen bonding, dicarboxylic acids have a tendency to form a hydrogen bonding network such as the one seen in a polypeptide chain. In the scheme, *N*-(2-mercaptopropionyl)glycine (MPG) is not a dicarboxylic acid, but has been selected because it is a simple amino acid, enabling wide applications in biology. Glutathione in the reduced form (GTR) is also a ubiquitous peptide found in organisms. Note that both these ligands are optically active. The size of a particle is controllable by the initial molar ratio of chloroaurate ion and ligands. With increase in the ligand contribution, size of particles reduces, because there are a larger number of ligands to cover the surface of the particle formed. This functional relation between size and the thiolate-to-metal content was precisely examined in the systems of AuMSA,[24] AgMSA[25] and PtMSA[28] (these terminologies refer to particles prepared with MSA as the surface modifier).

A typical reaction condition is as follows for a thiolate to aurate ion molar ratio of 2.0. Under vigorous stirring and ultrasonic irradiation, 80 mL of freshly prepared 0.3 M $NaBH_4$ aqueous solution was added to a water–methanol mixture containing 1 g of $HAuCl_4{\cdot}4H_2O$ and 0.73 g of MSA. After reduction, a flocculent precipitate was collected by decanting the supernatant solution and it was washed three times with water–methanol mixture (volume ratio of 1 : 3), by repeating the re-suspension–centrifugation process. The process was repeated three more times with 99.8% methanol to remove unbound MSA or AuMSA complexes. The resulting precipitate was dispersed in 15 mL distilled water and was dialyzed against a continuous flow of freshly distilled water for about 8 h. The suspension was dried by lyophilization and followed by evacuation on a vacuum line for 12 h. About 0.6 g of black powder was obtained finally.

Separation of particle size. Although we developed the phase separation method based on the solubility concept as a working hypothesis, we need careful consideration of the application of the concept to nanoscale materials. As the core

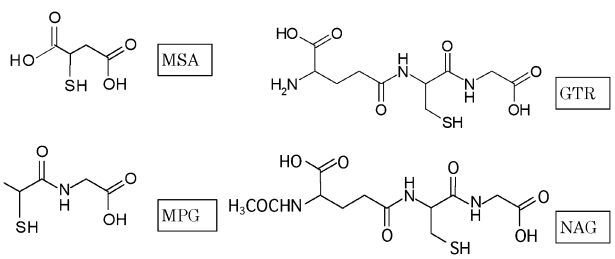

Scheme 1 Structural formulae of carboxylic acid related ligands.

of such a particle is hydrophobic and the shell part is hydrophilic, total solubility is regulated by the ratio of number of ligands to the total volume of the particle. We examined two solvent systems namely water–methanol and water–ethanol. Among them, the water–methanol system gave a reproducible and finely controllable result for Au, Ag and Pt nanoparticles. At a given water to methanol ratio, larger particles may precipitate and smaller particles remain in suspension until the size reaches the solubility limit, and finally all particles deposit to sediment. Thus, the phase separation method inherently sharpens the size distribution of the particles produced. This is very important to obtain a high quality crystal made of nanoparticles as monodispersity is the principal requirement of crystal formation. The best volume ratio of methanol to water is 10 : 3–4 as the solvent. The solubility of nanoparticles is the fundamental concept for size dependent extraction or deposition.[29,30]

As there is phase separation, particles are formed until all precursor species are consumed. The proposed reaction scheme of thiolate modified gold nanoparticles is shown in Scheme 2. It should be noted that stoichiometrically included water molecules act as staples. The ligand composition is proved by elemental analysis, TG and EDX.[24]

For small particles whose size is less than 2 nm, polyacrylamide gel electrophoresis (PAGE) is an effective technique for the separation of water dispersive gold clusters.[23,32–34] By the precise tuning of %T (T, total acrylamide concentration) and the gel conditions, one can separate different core size and differently modified particles from a mixture of clusters. The separated species can be extracted as successive bands. Fig. 1 illustrates this separation as a function of %T with band index figures varying from 3 to 9 for homogeneous gel conditions. This is very effective for the separation of gold clusters whose compositions such as $Au_{15}SR_{13}$ (hereafter, this is abbreviated as (15, 13)), (18, 14), (22, 16), (22, 17), (25, 18), (29, 20), (33, 22), (38, 24), (39, 24), (45, 25) and so forth may be determined by electrospray ionization mass spectrometry. This technique can be extended to nanometre-size clusters by using the gradient gel technique.[34] However, at present, its applicability is limited to particles whose core diameters are less than 1.5 nm for gold[34] and 2.5 nm for silver.[35] Beyond this size, the PAGE bands overlap severely, being unable to handle further separation. Applying more optimal experimental parameters and conditions, the PAGE technique will be more useful for the separation of larger particles exceeding 3 nm. Currently, transmission electron microscopy (TEM) is the main technique to determine the size of particles above this size regime.

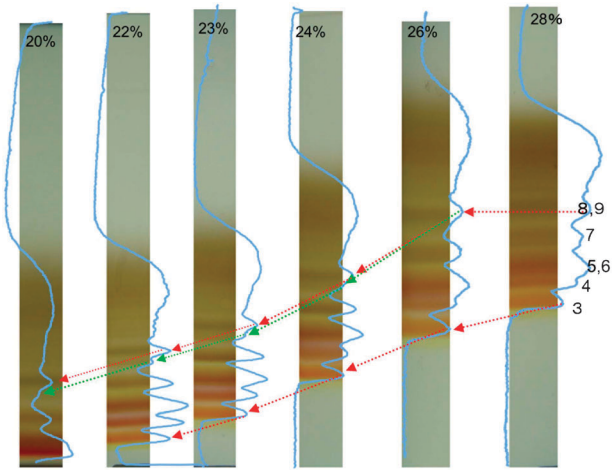

Fig. 1 Homogeneous gel PAGE pattern as a function of gel %T. Note that the band position shifts to lower direction when %T (denoted at the top of each column) decreases. The numbers at peaks on the right corner are band indices. Some overlapping bands, say 8 and 9 at 28%T, split at 22%T. Electrophoretic duration time was commonly 6 h at 150 V (from our unpublished data).

Surface modification and phase transfer. Regulation of inter-particle interactions is achieved in a tailored manner. Through suitable selection of a particular thiolate functional group, hydrophilicity, hydrophobicity, charge state, solubility and re-dispersibility in a given solvent can be designed at the molecular level. In the case of AuMSA nanoparticles, dried under vacuum and re-dispersed in water, the process could be repeated three times without any sign of coagulation. Reversible phase transfer of nanoparticles from aqueous solution to organic solvent or *vice versa* is also achieved by an appropriate selection of a surface modifying agent. It is known that hydrophilic ions such as carboxylates interact with oppositely-charged lyophilic ions through an electrostatic attraction, leading to highly hydrophobic ion-pairs as exemplified by a phase-transfer catalyst.[36] Such ion-pairs are produced stoichiometrically so as to extract into an organic phase from an aqueous phase. We emphasize that such reaction occurs between the "molecules". On the other hand, we have elucidated that the carboxylate-functionalized gold nanoparticles are well characterized as a regular molecular compound,[24] so that the hydrophilicity/hydrophobicity of such nanoparticles can be strictly controlled by molecular interaction of the carboxylate anions. Although nanoparticle extraction into an organic phase had already been reported,[37] extraction of "nanoparticles" based on ion-pair formation has

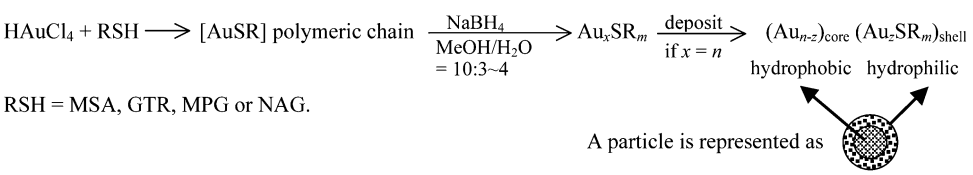

Scheme 2 Reaction scheme for formation of surface modified gold nanoparticles. Chloroaurate anions and thiolate form a polymeric complex chain as precursor species.[6,31] Au_xSR_m denotes a transient species, which finally changes to Au_nSR_m as a kinetically stabilized nanoparticle by deposition. A nanoparticle Au_nSR_m comprises a shell of Au_zSR_m and a core of Au_{n-z}. The subscript n is related to the critical size of a particle to deposit and z stands for the number of Au atoms in the shell part. The circle with crossed line represents the gold core and surrounding dotted part is the shell. Sometimes, a shell contains water molecules as staples for the ligands, MSA, GTR, MPG or NAG.

not been investigated in detail because the surfaces of nanoparticles have been poorly-defined. In the following, we describe the phase transfer of MSA-passivated gold nanoparticles across a water/oil interface by stoichiometric ion-pair formation between carboxylate anions and hydrophobic cations.

We used an AuMSA powder sample with 3.6 nm core-diameter as the starting material. The gold nanoparticles were surface-modified by MSA moieties of 8.6×10^{-4} mol per gram of the powder. Elemental analysis showed that the material contained 13.8 wt% MSA. When 2 mL of an aqueous AuMSA parent solution (5 mg per 20 mL) and 4 mL of a toluene solution of tetraoctylammonium bromide (TOABr) in a concentration range of 0.35–8.0 $\times$ 10^{-4} M were mixed, a dark-red color was transferred into the toluene phase, indicating that the gold nanoparticles moved from the aqueous phase to toluene across the water/toluene interface. After the evaporation of toluene, a dark-brown powder was obtained. The height of the 520 nm peak, corresponding to the surface plasmon of transferred gold dispersion, as a function of TOABr concentration shows that the absorption peak increased linearly with an increase in the TOABr concentration in the low TOA^+ region [plot is not shown; Ref. 29]. Since the ion-pair interaction is very strong in organic solvents, all TOA^+ species combine with MSA anions in the low TOA^+ concentration regime. With the known amount of TOA^+ and the extent of change in AuMSA from absorption measurements, we can derive a molar ratio of MSA to TOA^+. It showed that 0.53 of MSA ligands combined with one TOA species, implying that 0.95 of surface (COO^-) was bound to TOA.[29,38]

The carboxylic acid moiety of AgMSA can be easily esterified in *n*-butanol using sulfuric acid as a catalyst.[39] Thus the starting water-dispersible sols can be converted to oil-dispersible sols. In both cases, the conversion yield is more than 0.95, suggesting that these particles may be treated as typical chemical species.

(b) Structure of particle crystals

Environment dependent self-assembly. By careful combination of hydrophilicity (charged state of thiolate on nanoparticles) and hydrophobicity (charge neutrality of protonated thiolate) of the ligand, we can crystallize metallic nanoparticles at an air/water interface. Charged nanoparticles with the same sign are always repulsive in the bulk solution but can turn attractive at the interface where one part of the surface of the particle becomes neutral. Regulation of pH of the solution finely tunes this process through acid dissociation equilibrium. Note that particles are supplied from the bulk solution to the interface and hence they can be said to deposit at the air–liquid interface. Fig. 2(a–c) illustrates how the particles grow at the air/water interface to form a particle crystal (superlattice).[40] The model concludes that the SL growth is through the layer-by-layer step at an air–water interface, suggesting a smooth surface at the air-side (d) and the step structure at rear surfaces.[41] The existence of nanometre-sized steps on the surface of SLs is evident by an atomic force microscopic measurement as shown in (e).[42] The step height ranges from 3.5 nm to 4.3 nm, almost consistent with the size of particles, namely 3.5 nm.[43] Liquid is isotropic; *i.e.* density of the liquid is homogeneous and invariant for any amount of

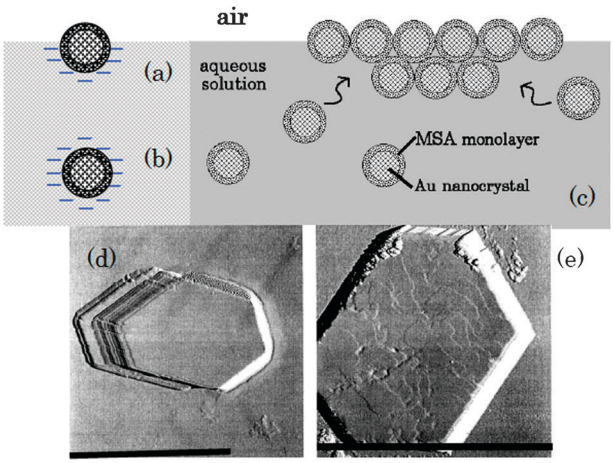

Fig. 2 Schematic images of superlattice formation at the interface. (a) Upper hemisphere is neutral at an interface. (b) Whole surface is negatively charged inducing strong repulsion in solution. (c) Particles in solution are isolated due to coulombic repulsion and those at the interface are deposited leading to crystallization.[40] (d) An atomic force microscopic image of the air-side shows a smooth surface and (e) the rear surface is covered with layer-by-layer steps. Scale bar = 2 μm.[41] Screw dislocation on the rear surface is observed in some cases (Ref. 42, not shown here).

reciprocal shift. Therefore, there is no lattice mismatch in the lateral direction when a crystal grows at the surface of a liquid in contrast to epitaxial growth on a solid substrate, giving strain-free crystals with flat surfaces. This creates almost freestanding crystals. This crystallization technique was effectively applied to form high quality SLs at an air/water interface for gold[43,44] and silver.[45]

From a different viewpoint, we can control a crystallization process by choosing the surrounding gaseous species, which interferes with the growth process. Fig. 3 presents the images of the effect of the surrounding gas on the self-assembly process observed by scanning electron microscopy (SEM)[46] together with the effect of temperature.[40] Keeping the total pressure of ambient gas at one atmospheric pressure at 25 °C, we observed three different morphologies of self-assembled structures as a function of ambient gas species such as (a) high-quality particle crystal with substantial platelet-like morphology in oxygen, nitrogen or air, (b) spherical aggregates in alkane or cycloalkane such as pentane, hexane, octane or cyclohexane and (c) irregular aggregates in acetonitrile or chloroform, that is polar gases. Energy dispersive X-ray (EDX) analysis shows that all these assemblies are made of nanoparticles. The morphological difference comes from a difference in the self-organization governing for the crystallization.[46] When the temperature increases to above 35 °C but below 40 °C in the case of (a), diffusion-limited aggregation of particles occurred (d) and above this temperature, all nanoparticles precipitate at the bottom of the vial [unpublished data].

Five-fold symmetry and high quality superlattices. When one carefully selects the crystal growth conditions and extends the growth period, we have high-quality SLs under an equilibrium growth condition.[43,44] Briefly, Au nanoparticle powder with 2 nm size was dispersed in distilled water to form brown

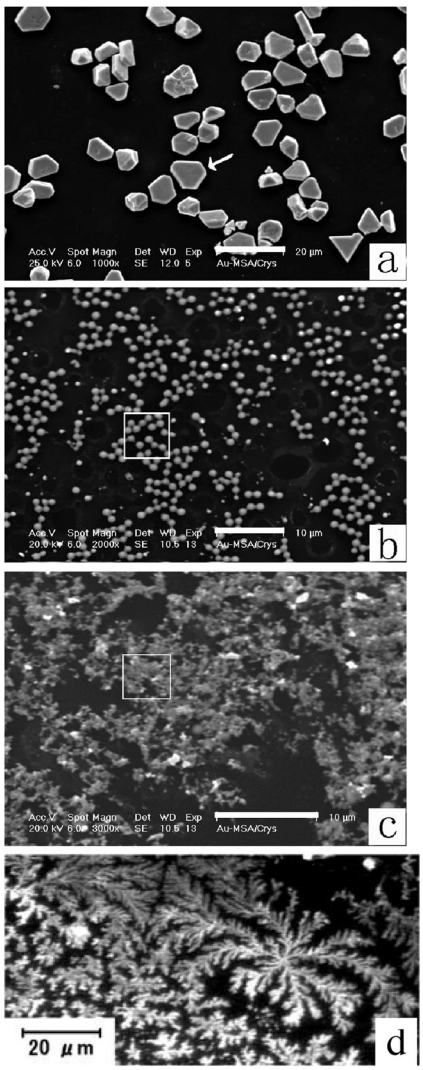

Fig. 3 Morphology regulation by ambient gas species (a for oxygen, nitrogen and air, b for pentane, hexane, octane and cyclohexane, c for acetonitrile and chloroform) at 25 °C and temperature (d at 35 °C) observed by SEM. Scale bar = 20 μm (a, d) and 10 μm (b, c). Inset rectangles in b and c show the EDX analysis area. Figures a, b, and c from Ref. 46 and d from Ref. 40. Permission from The Chemical Society of Japan, 2009.

suspensions with a mass concentration of *ca.* 2.0 mg mL^{-1}. Systematic acid concentration dependence on the SL formation was done in the HCl concentration range of 0.03 to 3 M and a better result was obtained at around 0.3 M. The optimal value varied with the amount of Au nanoparticle powder in the vial. Under the above conditions, the pH was 0.6. Then the solutions were filtered through a syringe-driven microfilter with 0.22 μm pore size and immediately stored in sealed glass vials to prevent the evaporation of the solvent. The glass vials were kept from apparent shaking and direct exposure to light. Within a week, crystallization started and gave numerous faceted SLs of micrometre sizes after several months. Sometimes, we observed SLs with five-fold-symmetry such as decahedron, Marks decahedron, and icosahedron shown in the top set of photographs of Fig. 4.[47] High resolution SEM clearly shows that an icosahedral SL is made up of 7.9 nm nanoparticles as shown in the lower expanded panel. The situation is the same as for other types of SLs. It is known that an icosahedral particle normally contains larger strain inside, due to the distortion of the inter-shell and intra-shell distances, so that this form could be present only for small sizes in metal nanoparticles. For example, the size limit of 27.35 nm has been obtained in icosahedral silver nanoparticles, whereas it is 273.3 nm in decahedra.[48,49] Note that the total number of silver atoms in an icosahedral nanoparticle of ~27 nm can be approximately estimated to be 4–5 × 10^5, corresponding to 40–50 shells.[50] Surprisingly, 1–2 × 10^8 nanoparticles are included in the SL of ~4 μm (Fig. 4) assuming that they are made of spheres of 7.9 nm in diameter, which correspond to 300–400 shells. This is probably due to the fact that a large relaxation of the internal strain caused by flexibility of the constituent nanoparticles makes the icosahedral structure much more stable. However, the strain remained in the structure could collapse the regular shape when handling the SL samples distributed at the air/solution interface (see one edge of icosahedron in Fig. 4).

However, in many cases examined, the structure of the SLs is *fcc* for AuNAG or *hcp* closest packing for AuMSA and AuMPG, giving six-fold symmetry. The highest-quality SL made of AuMSA showed clear preferential ordering within the SL.[51] Powder X-ray diffraction (XRD) shows a ring pattern due to random orientation of constituent crystallites on a glass or Si substrate. However, if random orientation is restricted by directional chemical bonding such as hydrogen bonding, the ring pattern changes to diffuse dots or crescent or even spot patterns. When we take the diffraction signal from a single SL, it will show the ring pattern in the case of random orientation of constituent particles within SL and shows a crescent pattern if component nanoparticles are aligned regularly. Based on the analysis of diffraction from a SL made of Au_{1709} with 15 × 6 truncated cuboctahedron shape that displayed distinct crescent patterns, we proposed a stacking structure for this SL and successfully explained both diffraction data from transmission electron diffraction (TED) and XRD.[51]

Faster crystallization. One of the drawbacks of the air–water interfacial method of synthesizing SLs is the time required for crystal formation. It takes several weeks to a couple of months for the formation of high quality SLs. For detailed examination and to find applications, the materials should be available in gram scale and the methods of such synthesis should be easily adaptable. In this context, we developed a new method at a liquid–liquid interface under a flowing nitrogen gas set-up as shown in Fig. 5.[52] Here the nanoparticles are dissolved in water and pH of the solution was adjusted as before.[44] To this acidic nanoparticle dispersion, 5 mL of toluene was added and the mixture was kept inside the set-up (stage 1). The paraffin oil-filled bubbler indicated a flow of two bubbles per second. The samples were left undisturbed for 2 days, in dark at a temperature below 25 °C. The SL formation started within a few hours at the toluene–water interface. Within 24 h, all the toluene evaporated and the SL films began to form on top of the aqueous layer (stage 2). A thick film with mirror like appearance was seen within 48 h, indicating the formation of gold nanoparticle SLs in micrometre dimensions (stage 3).

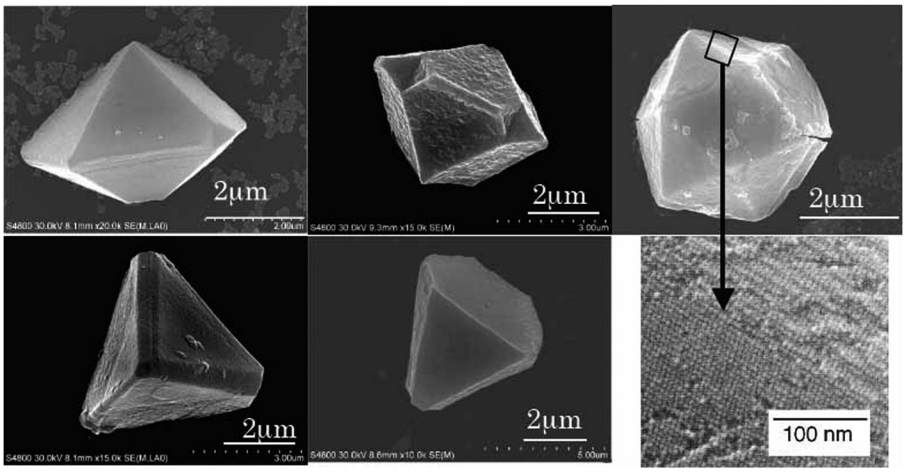

Fig. 4 SEM photos of 3D superlattice of AuNAG nanoparticles. From left to right; upper panels: decahedron, Marks decahedron, icosahedron (an expanded region of the icosahedron is shown below[47]). Note that an icosahedral SL comprises of constituent nanoparticles. Lower panels: tetrahedron, hexagonal pyramid in shape (unpublished data).

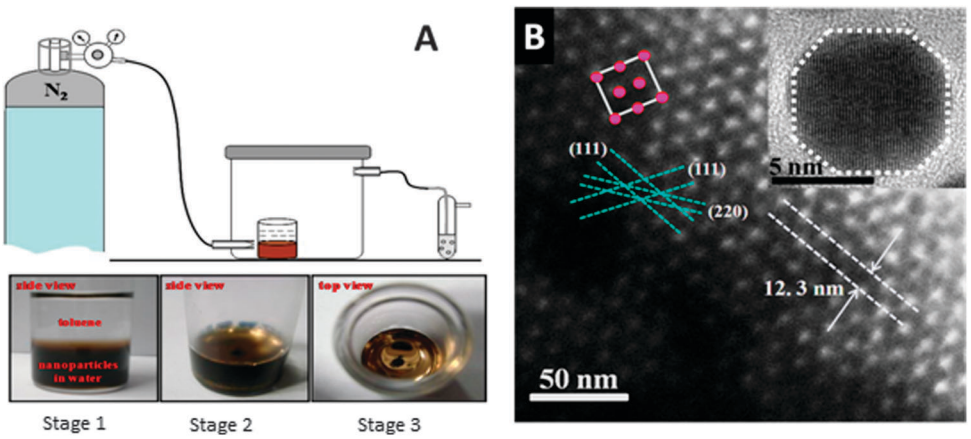

Fig. 5 (A) Cartoon representation of the setup used for the SL formation. The photographs show different stages of an SL formation (stage 1 and 2). The top view of the SL crystals (stage 3) clearly shows a continuous film at the interface. (B) HRTEM image of Au-SGAN. The inset of each figure shows the truncated octahedral (TO) shape of the nanoparticles with {100} and {111} facets. (Adapted from Ref. 52.).

Fig. 5B shows the HRTEM images of Au-SGAN fabricated by this rapid method. In both cases, the particles show a truncated octahedral (TO) shape with {100} and {111} facets which are shown in the insets of the figures. In the images, a $[110]_{SL}$ projection of the unit cell of the SL is represented by a rectangular box, where the subscript SL refers to the SL. Although the reason for the faster growth is not known, self-organization kinetics at the interface seems to be faster. Interfaces have shown to create faster superlattice structures as they make size separation possible.[53] Differences in the effect of interfacial potential on differently sized particles seems to be an important factor in effecting this size separation.

3. Functionality of crystals

Organized structures constructed with nanoparticles become useful only if they are functional. Functionality arises in terms of their physical or chemical properties which allow them to be used for specific applications. Among the properties, optical absorption and emission are most important. Properties of isolated nanoparticles such as plasmon resonance can be an important aspect and the effect of this on particle assembly has been investigated. Nanoparticles by themselves are very weakly luminescent with a quantum yield of 10^{-9} and in order to find observable emission from the structures, molecular fluorophores may be attached on them. Depending on the density of the fluorophores on the nanoparticle surface, the emission properties can be modified. Due to the proximity of metallic nanoparticles with large electron density, the fluorescence quantum yield of the fluorophores will be affected. Quenching is observed most prominently while metal enhanced emission has been reported in several nanoparticle systems. Packing of nanoparticles in SLs result in cavities which may be used for molecular incorporation. Molecules present in such environments will be subjected to electromagnetic fields induced by plasmon excitation of the particles. Such molecules may also be subjected to polarization by applied electric fields and all of these may be useful for sensing. The fact that nanoparticle systems can be conjugated with biomolecules and their interactions are highly

selective will enable the detection of such interactions using the concomitant variation in properties of SLs. From all these perspectives, functional SLs present numerous possibilities, some of which have been explored.

(a) Structure and properties of functional assemblies

Fluorescent superlattice. Glutathione protected nanoparticles have an $-NH_2$ and a –COOH group each. These can be used to make covalent functionalization on them. For example, if we are in need of a fluorophore on the ligands, we may attach a fluorescent marker by appropriate organic synthesis. The fluorophore can be tagged on the nanoparticle by different methods like exchange reaction of nanoparticles with fluorescent group labeled ligands. Nanoparticles can be synthesized directly using fluorescent molecule-tagged ligands. Assembly of such tagged nanoparticles will lead to fluorescent SLs. We developed fluorescent SLs using this approach. A fluorescein-based dye [5-((2-(and-3)-S-(acetylmercapto) succinoyl) amino) -fluorescein] conjugated mercaptosuccinic acid (SAMSA) was used to make nanoparticles along with free MSA ligands. Number of ligands per nanoparticle was calculated using the optical extinction coefficient of the ligands.[54] SL crystals were developed by the interfacial method. A similar method was used to develop dansylglutathione (DGSH) protected SLs as well. The crystals of Au-SGAN/SGD (containing both –SGD and *N*-acetylglutathione (–SGAN) ligands) nanoparticles result in principally two kinds of triangular morphologies, first one resembles a prism and second one is pyramidal with upper and lower surfaces having different areas. Moreover, it has a depression at the centre. We studied the unusual triangular morphology of SL crystals by SEM and confocal fluorescence microscopy. The results are comparable. Fig. 6(A–D) shows SEM and fluorescence images collected from two different triangular crystals of Au-SGD/SGAN SL.[55] Fig. 6(E–T) shows the confocal fluorescence images and corresponding overlay structure collected from the Au-SGD/SGAN SL triangle at a different depth. The green fluorescence is from the dansyl moiety. In one type of crystals, the fluorescence intensity is constant over the surface while in the other the intensity is maximum at the edges. This is due to the enhancement of the intensity at the edges in the latter case. The confocal images from crystal B support this preferential enhancement. The effect is not due to the confocal discrimination as fluorescence from the base is detectable (Fig. 6D).

Narrowing of surface plasmon absorption band. We examined the effects of ligand on the electronic state of SLs for three ligands, (a) MSA, (b) MPG and (c) NAG (see Scheme 1). High-resolution TEM (HRTEM) clearly shows that the SL consists of nanometre size particles (Fig. 7 left). As seen in the small-angle and wide-angle XRD (not shown here) and TED patterns, the assembly exhibits double periodicity. Small angle TED (SATED) is originating from atomic alignment on the 0.1 nm scale, and wide angle TED (WATED) is from the alignment of nanoparticles on the nm scale. It should be noted that crescent patterns appeared in WATED in the case of AuMPG and AuNAG SL. This suggests that there is preferential orientation in addition to translational ordering in the SL.[51] Images on the right (Fig. 7) also show the optical absorption spectra of three kinds of aggregation states: (i) dispersed in water, (ii) dried deposited aggregates on a quartz plate, and (iii) SL assemblies on a quartz plate for three thiolates. All dispersed nanoparticles exhibited small peaks at 2.2–2.4 eV corresponding to the surface plasmon resonance of gold particles.[56,57] As the nanoparticles densely assemble, the peaks red-shift and intensify. Such peak shifts can be explained using the classical theory of electronic polarizability using the

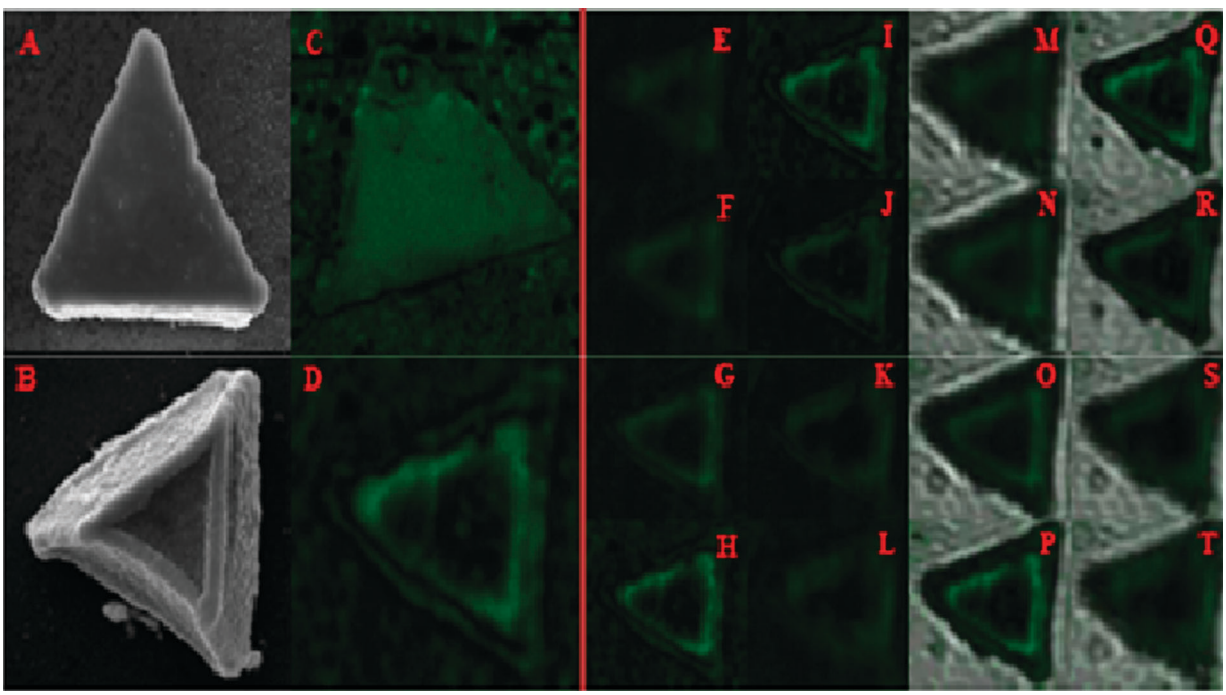

Fig. 6 (A–D) The two different morphological SLs of Au-SGAN/AGD and their corresponding fluorescence images. (E–T) The inverted confocal fluorescence images and corresponding overlay structure of the second type of triangle as a function of depth. (Adapted from Ref. 55.).

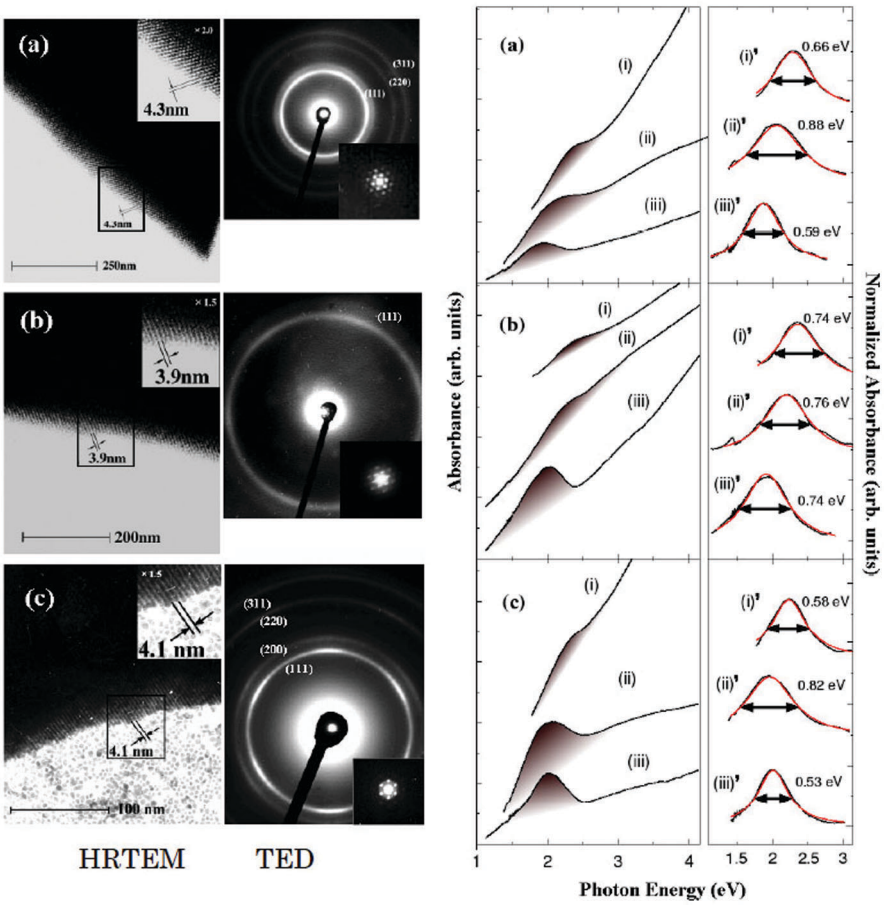

Fig. 7 Panel arrays from left to right are for HRTEM images, TED images, optical absorption spectra and those after subtraction of background for (a) AuMSA, (b) AuMPG and (c) AuNAG SLs. Inset in HRTEM is a magnified image of the boxed area. Inset in TED is small angle TED. Three spectra in the third and fourth columns are absorption spectra for (i) dispersion in water, (ii) deposited sample, and (iii) superlattices. Red lines are derived from the imaginary part of the dielectric function used with the parameters indicated in the figure. (Adapted from Ref. 57. Permission from American Institute of Physics, 2007.).

Thomson model.[56] Assuming that the nanoparticles are simple harmonic oscillators, the dielectric function of the SLs composed of these oscillators is given by a phenomenological equation with two fitting parameters, plasmon frequency and the damping factor, which is proportional to the line width. The best fit gave the red lines shown in Fig. 7. It is notable that the line width increases when the nanoparticles randomly assemble but decreases after forming a SL. It is impossible to explain this behavior within a classical theory. This observation resembles the coherent exciton migration in CuCl crystals or J-band formation in organic cyanine dye.[58] We emphasize that these properties are common to all three samples regardless of the differences in the ligand molecules. This is a requisite for high-quality SLs.

(b) Applications

Raman and electric current response to gas adsorption. One of the aspects of such solids is the fact that they are made of much larger units than typical crystals composed of atoms or ions. As a result, they are likely to have cavities which are also larger than those typically observed for regular crystals. Typical SLs are composed of particles of 8.5 nm core diameter. Considering a length of 0.7 nm for the MSA monolayer, the effective diameter of the particle including the monolayer is ~9.2 nm. This suggests that there are tetrahedral and octahedral voids of 1.04 and 1.90 nm radii, respectively. These pores are adequate to accommodate small molecules.[59] We decided to incorporate gases such as Ar, O_2, N_2 and CO_2 in these cavities and measure the effect of gas incorporation on the *I–V* (current–voltage) characteristics of the crystal (Fig. 8).[60] The bias voltage was 1.5 V. Till gas exposure, the system was in vacuum and at 300 s, the gas was exposed. At 600 s, the system was evacuated again. The response of the system recovers upon evacuation. As can be seen, the recovery is nearly complete. The incomplete recovery is due to adsorption within the SL and slow release of the gas. With extensive pumping, the system recovers completely. The process can be repeated again and again. The magnitude of response depends on the exposure and the type of gas. The incorporation of gases in SLs is expected to screen the electromagnetic interaction between the clusters. To see this effect, we decided to measure the Raman spectrum of a probe molecule, crystal violet (CV) incorporated in the SL, as a function of gas exposure. We see

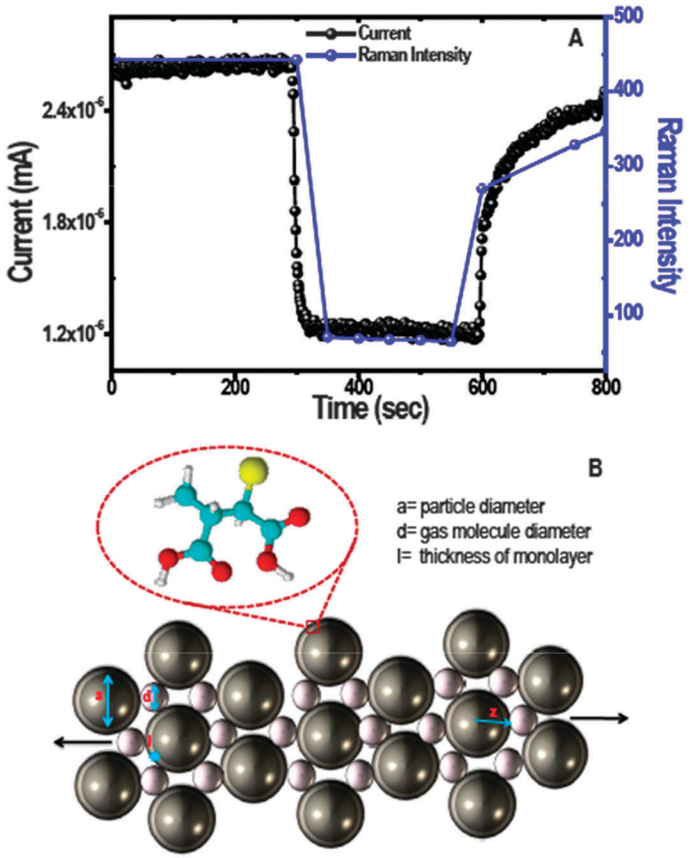

Fig. 8 (A) Comparison of change in Raman intensity of the 1170 cm^{-1} band of CV and current through an SL film upon exposure to CO_2, performed simultaneously. The Raman intensities have been scaled so that the data points are comparable with current. (B) Cartoon representation of gas molecules adsorbed on the surface of nanoparticles in SLs. The nanoparticles with the monolayer (shown separately) are shown by large spheres and the gas molecules are shown by small spheres in an idealized schematic. (Adapted from Ref. 60.).

that the Raman intensity of all the peaks of CV decreases with gas exposure and recovers completely upon evacuation. In Fig. 8A, we plot the Raman intensity of the 1170 cm^{-1} feature along with the current. Both follow the same trend. In Fig. 8A, the Raman intensities have been scaled to bring them to the same scale as current. Similar responses were found for the other bands too. The data suggest that Raman spectroscopy can also be used as a measure to study any phenomenon which can affect the change in properties of SLs. This is especially important in the case of noble metal nanoparticle SLs as these metals are surface enhanced Raman active which allow the measurement of small changes. Cartoon representation of gas molecules adsorbed on the surface of nanoparticles in SLs is shown in Fig. 8B. Simple electrostatics gives insight into the experimental observations. We calculate how the polarization in the medium is affected by that of the adsorbed gases. We consider for simplicity a situation, schematically shown in Fig. 8B, where a unit cell consists of a metal sphere of diameter a, representing a gold nanoparticle which is surrounded by a coating of monolayer of spatial extent l, followed by adsorbed gas molecules of diameter d. The electrodes are infinitely removed along the z-axis, generating a uniform external electric field, E_0, parallel to the z-axis. The polarization of the monolayer protected gold nanoparticles is given by $a^3 \hat{A} Æ_C[(Æ\hat{A}_N - Æ\hat{A}_C)/(Æ\hat{A}_N + 2\,Æ_C)]\,E_0$; $Æ\hat{A}_N$ and $Æ\hat{A}_C$ are the dielectric constants of the nanoparticle and the monolayers. For a metal, the dielectric constant can be taken to diverge, $Æ_N \gg Æ\hat{A}_C$,[61] in which case the polarization dipole due to the metal sphere is simply given by $(a^3\, Æ\hat{A}_C/2)\,E_0$. The polarization is large for spheres of size of a few nanometres. The polarization field modifies the local field in the system. The electric field at a point (r, θ) is given by $E\,(r, \theta) = E_0 \cos(\theta)\,(1 - a^3\, Æ_C/2\, r^3)$. The gas molecule adsorbed in the system is polarized by this modified electric field. Let us consider the situation close to the z-axis for simplicity. The polarized dipole moment of the adsorbed molecule produces an extra electric field that opposes this local electric field, and is given by $p = \alpha E_{pol}$ where E_{pol} is the polarization field, E at $r = a/2 + l + d/2$. We set $\cos(\theta) = 1$ for the electric field along the z-axis. α is the polarizability of the gas molecule. Considering the contribution due to the polarizations of n such adsorbed molecules in the vicinity of the nanoparticle, we get the net electric field given by $E_{net} = E(r = z, \theta = 0) - 3\,np\,Æc/[z^3\,(2 + Æc)]$. The second term is due to the extra polarization of the adsorbed molecules that opposes the existing electric field and is proportional to the polarizability of the adsorbed molecule. The Raman intensity depends on the local electric field, E_{net}.

Design of high *k* dielectric materials. Granular metal films, in which metal nanocrystals are dispersed in an insulator, are interesting electronic materials owing to their unique physical properties, such as the negative temperature coefficient of

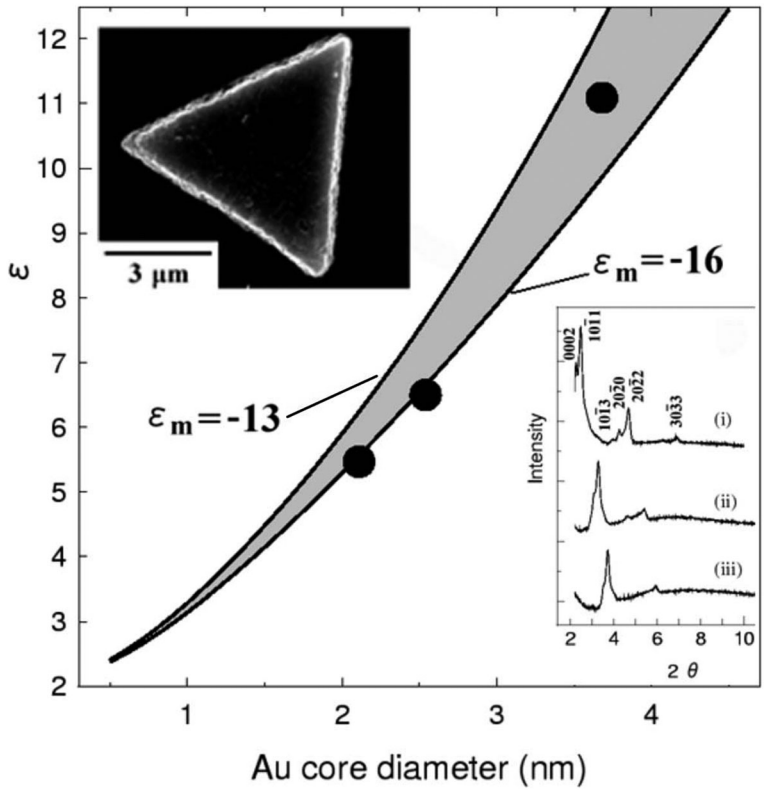

Fig. 9 Optical dielectric constants as a function of Au core size. The dots show the dielectric constant from the experimental refractive indices. The curves are calculated using the Thomson model with dielectric constants for gold particle and MSA. Insets show the SEM micrographic image of SL and the SAXRD of three samples, 3.11, 3.54 and 4.68 nm, which identify the crystalline form of the samples. (Adapted from Ref. 65, Permission from The Japan Society of Applied Physics, 2010.).

electric conductivity and a high permittivity.[62] These properties are potentially useful in increasing electronic device density and suppressing thermal runaway due to the positive feedback of increase in temperature and conductivity. To obtain these unique properties, the metal content of the films should preferably be higher than ~20%. However, as the nanocrystal density increases, the adjacent nanocrystals become connected in the films with metal contents higher than ~10%. This eliminates a wide range of applications owing to the damping of surface plasmon and electric leakage.

One material with the potential to satisfy both the high metal content and the isolation of nanocrystals is a metallic nanoparticle SL as has been mentioned already.[1,2,7,43,63] Since gold nanoparticles with organic moiety can be regarded as composite materials (a particle in Scheme 2), we can design a new class of dielectric materials at the molecular level. The metallic content can be tuned both by (1) changing the diameter of the metal with constant ligand, and by (2) choosing the length of the thiolate residue with the same core size. The interparticle distance can be designed to be ~1 nm by selecting short surfactant molecules.[57] Since MSA is one of the shortest chain-length thiolate, change of thiolate causes lowering of the dielectric constant and is not good for high k materials. Note that there is no leakage even though the insulating layer thickness is extremely thin at 1 nm. Also, the size distribution of the constituent nanocrystals is spontaneously narrowed during SL growth,[64] which makes the closest packing of the metal nanocrystals possible. Therefore, it is important to know what happens if we measure the dielectric constant of the SL shown in Fig. 4.

In AuMSA SLs, the thiolate is fixed with a molecular length of ~0.6 nm, but core sizes are different. From the small angle XRD (SAXRD) data, we can determine the lattice constant a of a *hcp* motif, that gave a = 3.11, 3.54 and 4.68 nm, respectively, corresponding to the filling factors of 0.23, 0.27 and 0.36. The refractive indices of the SLs were evaluated by the ratio of the geometrical height to optical height obtained by laser microscopy at the wavelength of 685 nm. Note that the lateral dimension of samples is of the order of micrometres. This means that we can map out the topography of very thin films consisting of different dielectric substances. The optical dielectric constant for each lattice is given by the square of the refractive indices. Fig. 9 is a plot of the optical dielectric constant against the Au core diameter, considering the thickness of the shell to be 0.5 nm.[65] Calculated curves are from Maxwell–Garnett theory using permittivity of metal particles to be from −13 to −16 due to diversity of the values in the literature,[66–68] and considering the dielectric constant of MSA to be 2.10. Using the above parameters, the Au core size dependence of the permittivity was well reproduced by a classical theory, which predicts that the dielectric constant of SL made of particles with a core diameter of 12 nm exceeds 1000. It is apparent that the dielectric constant of these composite materials is tuned by controlling the Au core size.

4. Conclusions and outlook

Periodic assemblies of monolayer protected noble metal nanoparticles are new types of solids. Hydrogen bonding induced assembly of such nanoparticles can be made by the proper choice of monolayer and conducting the assembly at a solution–air interface in acidic solutions. The crystal growth happens from the isotropic solution phase and particle assembly proceeds in a step-by-step fashion at the interface. The crystals show double periodicity; Angstrom scale in the case of atoms and nanometre scale in the case of the particles. The assemblies show five-fold-symmetry occasionally, arising from the formation of multiply twinned SLs. When all the particles of the SLs are aligned translationally and orientationally, the surface plasmon band reveals distinct narrowing similar to motional narrowing of exciton migration found only in high quality crystals. When the lattices align poorly, the diffraction spots due to the crystal are smeared. The SLs exhibit mostly cubic close packing, with nanometre scale cavities, which can incorporate small molecules. Exposure of the SLs to gases leads to reduction in electrical conductance of the crystals and the change in inter-particle interaction can be seen in Raman spectra of the spectroscopic labels.

Superlattices of noble metal nanoparticles belong to a sub-class of nanoparticle assembled materials; diverse categories of these belonging to semiconducting, magnetic, insulating, anisotropic and other nanoparticles are being investigated extensively. Our studies show that interfacial method allows the growth of well-defined crystals by controlling the interactions between the monolayers. The materials so derived can be provided with functional attributes such as fluorescence and the porosity of the materials may be used for sensing. The application of such assembled solids for high k dielectrics is interesting. Although the structure of the materials is clear, the mechanism of growth at the interface needs more clarity and time dependent measurements of the interface and probing the process from the liquid side is required.

The creation of macroscopic quantities of these materials in shorter time and the possibility to modify their properties by varying parameters of the core and the monolayer would bring in new possibilities. The fact that the cavities in them can be tuned will enable the creation of new sensors. Spectroscopic sensing of the properties of SLs as has been demonstrated using Raman spectroscopy is a new avenue. Mixed SLs of different metals as well as between metals and semiconductors present another way to tune the properties of the assembled solids. Complexity in nanoparticles synthesized currently will be reflected in SLs as well and these new assembled solids with various kinds of nanoparticle cores and functional molecular bridges will surely produce novel artificial solids. One area of attention could be SLs of alloy nanoparticles. Newer functional solids with stimulus-responsive monolayers such as those with photoresponsive molecules will make functional materials. Many excitements happening today in small, sub-nanometre clusters of noble metals will be reflected in SLs also in the near future.

Acknowledgements

KK acknowledges financial support (A: 09304068, S: 16101003) by MEXT. The nanoparticle research program of TP is supported by the Department of Science and Technology, Government of India. We thank all our co-workers whose work made it possible to write this perspective. Research support through a bilateral grant (JSPS, Japan-DST, India) made it possible to pursue many of the ideas presented here.

References

1 C. P. Collier, T. Vossmeyer and J. R. Heath, Nanocrystal superlattices, *Annu. Rev. Phys. Chem.*, 1998, **49**, 371–404.
2 C. B. Murray, C. R. Kagan and M. G. Bawendi, Synthesis and characterization of monodisperse nanocrystals and close- packed nanocrystal assemblies, *Annu. Rev. Mater. Sci.*, 2000, **30**, 545–610.
3 R. L. Whetten, J. T. Khoury, M. M. Alvarez, S. Murthy, I. Vezmar, Z. L. Wang, P. W. Stephens, C. L. Cleveland, W. D. Luedtie and U. Landman, Nanocrystal gold molecules, *Adv. Mater.*, 1996, **8**, 428–433.
4 M. P. Pileni, Nanocrystal self-assemblies: Fabrication and collective properties, *J. Phys. Chem.*, 2001, **105**, 3358–3371.
5 M. Brust, J. Fink, D. Bethell, D. J. Schiffrin and C. J. Kiely, Synthesis and reactions of functionalised gold nanoparticles, *J. Chem. Soc., Chem. Commun.*, 1995, 1655–1656.
6 A. C. Templeton, W. P. Wuelfing and R. W. Murray, Monolayer-protected cluster molecules, *Acc. Chem. Res.*, 2000, **33**, 27–36.
7 S. Sun and C. B. Murray, Synthesis of monodisperse cobalt nanocrystals and their assembly into magnetic superlattices, *J. Appl. Phys.*, 1999, **85**, 4325–4330.
8 E. Shevchenko, D. Talapin, A. Kornowski, F. Wiekhorst, J. Kötzler, M. Haase, A. Rogach and H. Weller, Colloidal crystals of monodisperse FePt nanoparticles grown by a three-layer technique of controlled oversaturation, *Adv. Mater.*, 2002, **14**, 287–290.
9 M. L. Steigerwald and L. E. Brus, Semiconductor crystallites: A class of large molecules, *Acc. Chem. Res.*, 1990, **23**, 183–188.
10 L. Brus, Capped nanometer silicon electronic materials, *Adv. Mater.*, 1993, **5**, 286–289.
11 C. B. Murray, C. R. Kagan and M. G. Bawendi, Self-organization of CdSe nanocrystallites into three-dimensional quantum dot superlattices, *Science*, 1995, **270**, 1335–1338.
12 D. V. Talapin, E. V. Shevchenko, A. Kornowski, N. Gaponik, M. Haase, A. L. Rogach and H. A. Weller, A new approach to crystallization of CdSe nanoparticles into ordered three-dimensional superlattices, *Adv. Mater.*, 2001, **13**, 1868–1871.
13 S. Sato, N. Yamamoto, K. Nakanishi, H. Yao, K. Kimura, T. Narushima, Y. Negishi and T. Tsukuda, Self-assembly of Si clusters into single crystal arrangements: Formation of Si10 cluster crystals, *Jpn. J. Appl. Phys.*, 2003, **42**, L616–L618.
14 S. Sato, H. Yao and K. Kimura, Self-assembly of Si nanoparticles: Emergence of two-dimensional Si nanoparticle lattices, *Jpn. J. Appl. Phys.*, 2004, **43**, L927–L929.
15 E. V. Shevchenko, D. V. Talapin, N. A. Kotov, S. O'Brien and C. B. Murray, Structural diversity in binary nanoparticle superlattices, *Nature*, 2006, **439**, 55–59.
16 Y. Yang and K. Kimura, Surface charge driven size evolution during the formation of self-assembled nanostructures from discrete hydrophilic silver nanoparticles, *Nanotechnology*, 2007, **18**, 465603.
17 B. Nikoobakht, Z. L. Wang and M. A. El-Sayed, Self-assembly of gold nanorods, *J. Phys. Chem. B*, 2000, **104**, 8635–8640.
18 M. P. Pileni, Control of the size and shape of inorganic nanocrystals at various scales from nano to macrodomains, *J. Phys. Chem. C*, 2007, **111**, 9019–9038.
19 P. R. Sajanlal, T. S. Sreeprasad, A. K. Samal and T. Pradeep, Anisotropic nanomaterials: Structure, growth, assembly and functions, *Nano Rev.*, 2011, **2**, 5883, DOI: 10.3402/nano.v2i0. 5883.
20 K. Kusaka, N. Wada and A. Tasaki, Magnetic properties of ferromagnetic metal alloy fine particles prepared by evaporation in inert gases, *Jpn. J. Appl. Phys.*, 1969, **8**, 599–605.
21 J. Turkevich, P. Stevenson and A. Hillier, Study of the nucleation and growth processes in the synthesis of colloidal gold, *J. Discuss. Faraday Soc.*, 1951, **58**, 55–75.
22 M. Brust, M. Walker, D. Bethell, D. J. Schiffrin and R. Whyman, Synthesis of thiol-derivatised gold nanoparticles in a two-phase liquid–liquid system, *J. Chem. Soc., Chem. Commun.*, 1994, 801–802.

23 T. G. Schaaff and R. L. Whetten, Giant gold–glutathione cluster compounds: Intense optical activity in metal-based transition, *J. Phys. Chem. B*., 2000, **104**, 2630–2641.
24 S. Chen and K. Kimura, Synthesis and characterization of carboxylate-modified gold nanoparticle powders dispersible in water, *Langmuir*, 1999, **15**, 1075–1082.
25 S. Chen and K. Kimura, Water soluble silver nanoparticles functionalized with thiolate, *Chem. Lett*., 1999, 1169–1170.
26 A. Taleb, C. Petit and M. P. Pileni, Synthesis of highly monodisperse silver nanoparticles from AOT reverse micelles: Away to 2D and 3D Self-Organization, *Chem. Mater*., 1997, **9**, 950–959.
27 M. Brust, D. Bethell, D. J. Schiffrin and C. J. Kiely, Novel gold-dithiol nano-networks with non-metallic electronic properties, *Adv. Mater*., 1995, **7**, 795–797.
28 S. Chen and K. Kimura, Synthesis of thiolate-stabilized platinum nanoparticles in protolytic solvents as isolable colloids, *J. Phys. Chem. B*, 2001, **105**, 5397–5403.
29 H. Yao, O. Momozawa, T. Hamatani and K. Kimura, Phase transfer of gold nanoparticles across a water/oil interface by stoichiometric ion-pair formation on particle surfaces, *Bull. Chem. Soc. Jpn*., 2000, **73**, 2675–2678.
30 S. Chen, H. Yao and K. Kimura, Reversible transference of Au nanoparticles across the water and toluene interface: A Langmuir type adsorption mechanism, *Langmuir*, 2001, **17**, 733–739.
31 T. G. Schaaff, M. N. Shafigullin, J. T. Khoury, I. Vezmar, R. L. Whetten, W. G. Cullen, P. N. First, C. Gutierrez-Wing, J. Ascensio and M. J. Jose-Yacaman, Isolation of smaller nanocrystal Au molecules: Robust quantum effects in optical spectra, *J. Phys. Chem. B*, 1997, **101**, 7885–7891.
32 Y. Negishi, Y. Takasugi, S. Sato, H. Yao, K. Kimura and T. Tsukuda, Magic-numbered Aun clusters protected by glutathione monolayers (n = 18, 21, 25, 28, 32, 39): Isolation and spectroscopic characterization, *J. Am. Chem. Soc*., 2004, **126**, 6518–6519.
33 Y. Negishi, K. Nobusada and T. Tsukuda, Glutathione-protected gold clusters revisited: Bridging the gap between gold(1)-thiolate complexes and thiolate-protected gold nanocrystals, *J. Am. Chem. Soc*., 2005, **127**, 5261–5270.
34 K. Kimura, N. Sugimoto, S. Sato, H. Yao, Y. Negishi and T. Tsukuda, Size determination of gold clusters by polyacrylamide gel electrophoresis in a large cluster region, *J. Phys. Chem. C*, 2009, **113**, 14076–14082.
35 Y. Yang and K. Kimura, Highly ordered superlattices from polydisperse Ag nanoparticles: A comparative study of fractionation and self-correction, *J. Phys. Chem. B*, 2006, **110**, 24442–24449.
36 C. M. Starks and C. Liotta, *Phase Transfer Catalysis, Principles and Techniques*, Academic Press, London, 1978, ch. 4.
37 H. Hirai and H. Aizawa, Preparation of stable dispersions of colloidal gold in hexanes by phase transfer, *J. Colloid Interface Sci*., 1993, **161**, 471–474.
38 H. Yao, O. Momozawa, T. Hamatani and K. Kimura, Stepwise size-selective extraction of carboxylate-modified gold nanoparticles from an aqueous suspension into toluene with tetraoctylammonium cations, *Chem. Mater*., 2001, **13**, 4692–4697.
39 J. Tominaga, S. Sato, H. Yao and K. Kimura, Esterification of surface modified silver nanoparticles with *n*-butanol, *Chem. Lett*., 2002, 950–951.
40 S. Sato, S. Wang, S. Kinugasa, H. Yao and K. Kimura, *Nanocluster superlattices grown at solution surfaces*, *Physics, Chemistry and Application of Nanostructures*, ed. V. E. Borisenko, S. V. Gaponenko and V. S. Gurin, World Scientific, 2003, pp. 313–319.
41 We thank Drs Katsuya Honda & Masamichi Ishikawa (MRI) for the AFM measurement of AuMSA superlattices.
42 H. Yao, S. Sato and K. Kimura, *Self-assembling of gold nanoparticles at an air/water interface*, in *Nanoparticle Assemblies and Super-structures*, ed. N. A. Kotov, CRC Press, 2005, pp. 601–614.
43 K. Kimura, S. Sato and H. Yao, Particle crystals of surface modified gold nanoparticles grown from water, *Chem. Lett*., 2001, 372–373.
44 S. Wang, S. Sato and K. Kimura, Preparation of hexagonal-close-packed colloidal crystals of hydrophilic monodisperse gold nanoparticles in bulk aqueous solution, *Chem. Mater*., 2003, **15**, 2445–2448.
45 Y. Yang, S. Liu and K. Kimura, Superlattice formation from polydisperse Ag nanoparticles by a vapor-diffusion method, *Angew. Chem., Int. Ed*., 2006, **45**, 5662–5665.
46 S. Wang, S. Sato and K. Kimura, Influence of organic vapors on the self-assembly of gold nanoparticles at solution-gas interfaces, *Chem. Lett*., 2003, 520–521.
47 H. Yao, T. Minami, A. Hori, M. Koma and K. Kimura, Fivefold symmetry in superlattices of monolayer-protected gold nanoparticles, *J. Phys. Chem. B*, 2006, **110**, 14040–14045.
48 S. Ino, Stability of multiply-twinned particles, *J. Phys. Soc. Jpn*., 1969, **27**, 941–953.
49 F. Baletto and R. Ferrando, Structural properties of nanoclusters: Energetic, thermodynamic and kinetic effects, *Rev. Mod. Phys*., 2005, **77**, 371–423.
50 S. C. Hendy and J. P. K. Doye, Surface-reconstructed icosahedral structures for lead clusters, *Phys. Rev. B: Condens. Matter*, 2002, **66**, 235402.
51 S. Sato, S. Wang and K. Kimura, Atomic alignment in particle crystals of Au nanoparticles grown at an air/water interface, *J. Phys. Chem. C*, 2007, **111**, 13367–13371.
52 E. S. Shibu, K. Kimura and T. Pradeep, Gold nanoparticle superlattices: Novel surface enhanced Raman scattering active substrates, *Chem. Mater*., 2009, **21**, 3773–3781.
53 T. U. B. Rao and T. Pradeep, Luminescent Ag_7 and Ag_8 Clusters by Interfacial Synthesis, *Angew. Chem., Int. Ed*., 2010, **49**, 3925–3929.
54 N. Nishida, E. S. Shibu, H. Yao, T. Oonishi, K. Kimura and T. Pradeep, Fluorescent gold nanoparticle superlattices, *Adv. Mater*., 2008, **20**, 4719–4723.
55 E. S. Shibu, M. A. H. Muhammed, K. Kimura and T. Pradeep, Fluorescent superlattices of gold nanoparticles: A new class of functional materials, *Nano Res*., 2009, **2**, 220–234.
56 S. Sato, H. Yao and K. Kimura, Optical absorption properties of three-dimensional Au nanoparticle crystals, *Chem. Lett*., 2002, 526–527.
57 T. Oonishi, S. Sato, H. Yao and K. Kimura, Three-dimensional gold nanoparticle superlattices: Structures and optical absorption characteristics, *J. Appl. Phys*., 2007, **101**, 114314–114318.
58 C. Duschl, M. Lösche, A. Miller, A. Fischer, H. Möhwald and W. Knoll, Two-dimensional crystals of J-band-forming cyanine dye, *Thin Solid Films*, 1985, **133**, 65–72.
59 S. Wang, S. Sato, H. Yao and K. Kimura, Inclusion-water-cluster in a three-dimensional superlattice of gold nanoparticles, *J. Am. Chem. Soc*., 2004, **126**, 7438–7439.
60 E. S. Shibu, J. Cyriac, T. Pradeep and J. Chakrabarti, Gold nanoparticle superlattices as functional solids for concomitant conductivity and SERS tuning, *Nanoscale*, 2011, **3**, 1066–1072.
61 J. D. Jackson, *Classical Electrodynamics*, Wiley Eastern Ltd, New Delhi, 1982.
62 I. S. Beloborodov, A. V. Lopatin, V. M. Vinokur and K. B. Efetov, Granular electronic systems, *Rev. Mod. Phys*., 2007, **79**, 469–518.
63 S. I. Stoeva, B. L. V. Prasad, S. Uma, P. K. Stoimenov, V. Zaikovski, C. M. Sorensen and K. J. Klabunde, Face-centered cubic and hexagonal closed-packed nanocrystal superlattices of gold nanoparticles prepared by different methods, *J. Phys. Chem. B*, 2003, **107**, 7441–7448.
64 S. Sato, H. Yao and K. Kimura, Equilibrium growth of three-dimensional gold nanoparticle superlattices, *Physica E*, 2003, **17**, 521–522.
65 S. Sato, T. Ito and K. Kimura, Refractive index regulation of gold nanocrystal superlattices by varying the nanocrystal size, *Jpn. J. Appl. Phys*., 2010, **49**, 06GJ05.
66 G. B. Irani, T. Huen and F. Wooten, Optical properties of gold and α-phase gold-aluminum alloys, *Phys. Rev. B: Solid State*, 1972, **6**, 2904.
67 P. B. Johnson and R. W. Christy, Optical constants of the noble metals, *Phys. Rev. B: Solid State*, 1972, **6**, 4370.
68 E. D. Palik, *Handbook of Optical Constants of Solids*, Academic, New York, 1985.